



# Identifying Rock Loads on TBM Shields During Standstills (Non-Advance-Periods)

Paul J. Unterlass · Georg H. Erharter · Thomas Marcher

Received: 3 November 2020 / Accepted: 31 July 2022 / Published online: 21 August 2022  
© The Author(s) 2022

**Abstract** Tunnel boring machine (TBM) operational data is mostly analysed with respect to data that was recorded during the advance of the TBM. Focusing on data that was recorded during standstills of a gripper TBM, we analyse rock loads that were passively recorded in the cylinders of a small roof support shield. These roof support cylinders are situated beneath the TBM's shield – extending it against the rock mass during non-advance periods. Equipped with pressure sensors, they enable the unique opportunity of logging rock load variations throughout the tunnel. Hence due to the big amount of resulting data, techniques of unsupervised machine learning (i.e. cluster analysis) are used to automatically pre-process the TBM operational data. Furthermore, regression analysis is used to determine sections of the tunnel where rock loads are mainly occurring on the left or right side respectively. The data driven analysis shows that the main rock loads are occurring on the right side of the TBM which is in good accordance with observation from the construction site, as well as numerical models from literature. This paper contributes towards the understanding of rock load conditions in anisotropic rock masses recorded during the drive of a deep hard rock tunnel.

**Keywords** Rock load · Machine learning · Anisotropy · Stress redistribution · TBM non-advance-data · Load on TBM shields

## Abbreviations

TBM	Tunnel boring machine
ML	Machine learning
RSC	Roof support cylinders
ET	Exploratory tunnel
GI	Geological indication (rockmass behaviour classification system)
BBT	Brenner base tunnel
OPTICS	Ordering points to identify the clustering structure
LIP	Line of isotropic pressure

## 1 Introduction

Remote rock load monitoring is of increasing importance in mechanized tunnelling. It allows tunnel boring machine (TBM) operators, engineering geologists and geotechnical engineers to collect, store and process information about the load acting at the interface between TBM shield and the surrounding rock mass, a region that cannot be observed by other expeditious means. Important not only in consideration of squeezing ground conditions as intensively studied by (Ramoni, 2010; Ramoni and Anagnostou, 2006, 2010a, 2010b, 2011), but furthermore in terms of the deformation

---

P. J. Unterlass (✉) · G. H. Erharter · T. Marcher  
Institute of Rock Mechanics and Tunnelling, Graz  
University of Technology, Rechbauerstraße 12, 8010 Graz,  
Austria  
e-mail: unterlass@tugraz.at

behaviour and stress redistribution of anisotropic, schistose rock masses in a deep hard rock tunnel. To tickle out relevant information of the collected TBM operational data, application of digital systematic data analysis is inevitable. Analysis of operational data has shown a rapid increase in the recent decade, amongst others due to a successful implementation of modern, digital techniques such as Machine Learning (ML) in tunnelling (Marcher et al. 2020a). However, most of these successfully implemented methods, respectively recently published papers only consider data that was recorded during TBM advance: e.g. (Festa et al. 2012) focus on the shield – ground interaction in soft rock tunnelling; (Bach et al. 2018) propose a new contractual advance classification based on TBM advance data; (Erharter et al. 2019a; 2019b; 2020) show that TBM operational data can be successfully used as input for supervised ML based rock mass behaviour classification. Furthermore, only few authors (e.g. Entacher et al. 2012; Huang et al. 2018; Li et al. 2011; Sun et al. 2018) successfully applied those modern techniques on TBM operational data concerning loading situations. Pilgerstorfer et al. 2011 did a comparable study to determine the deformability of the rock mass by conducting in-situ plate load tests in a hard rock tunnel and most recently Marcher et al. (2020b) use the grippers of an open TBM to perform loading tests onto the rock mass, focused on data logged during standstills of the machine.

The present paper reports on systematic data analysis of non-advance data from an open gripper TBM that excavated the exploratory tunnel (ET) Ahrental Pfons of the Brenner Base Tunnel (BBT) (“BBT-SE.com,” 2020). This gripper machine is equipped with a roof support shield directly behind the cutterhead (Figs. 1 and 2) which for safety reasons is extended against the tunnel wall during standstills (for details see chapter 2.1). The roof support shield is driven by two separate cylinders—left and right, placed approximately two meters apart—which can be controlled individually. Sensors separately record the pressure that acts on both sides of the TBM’s roof support shield. This provides the unique opportunity to analyse differential rock-loads that are applied to each side of the shield. Hence, this study enables all parties involved in the tunnel construction process a fast way to collect, store and process valuable information

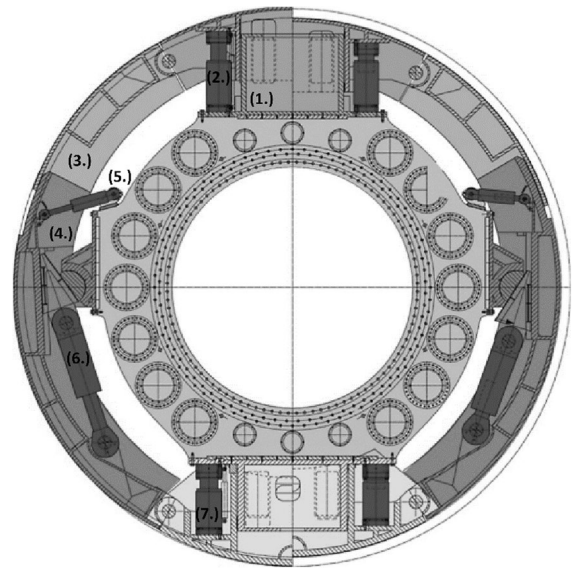


**Fig. 1** Cross section of the gripper TBM in the shield area, right behind the cutterhead. (1.) Left part of the roof supporting shield. (2.) Left roof supporting cylinder. (3.) Upper side panel, (4.) lower side panel. (5.) Recoiling /cylinder, (6.) wedge cylinder and (7.) floor cylinder. The same arrangement of instruments counts for the right side of the cross section. (modified after Flora et al. 2019; source: Herrenknecht AG)

to evaluate the deformation behaviour and stress redistribution of anisotropic, schistose rock masses in a deep hard rock tunnel.

In chapter 2, a short overview on the origin and nature of the investigated data is given, in chapter 3 the methodologies of data logging, pre-processing and investigation are presented, before showing first results on the shield—rock mass interaction in chapter 4. Finally, in chapter 5 the results will be discussed and, in the end, a short conclusion/outlook is given.

## 2 Background

### 2.1 BBT Exploratory Tunnel Ahrental-Pfons and TBM Specifics

As part of the Brenner Base Tunnel (BBT), a continuous exploratory tunnel (ET) is excavated along the entire length and ahead of the two parallel main tunnels (Bergmeister 2019). The ET Ahrental-Pfons in particular comprises a 16.7 km long section of the entire ET driven from the Austrian side towards

**Fig. 2** Side view on the gripper TBM used during construction of the exploratory tunnel Ahrental-Pfons. (“bbtinfo.eu,” 2020)



South. The first 15 km of this section are considered in our analysis. As the purpose of the tunnel is to investigate the geological and geotechnical conditions on site, intensive work has been undertaken to analyse different machine parameters from the TBM and their response towards the rock mass (Bergmeister and Reinhold 2017). Gained knowledge is then transferred to the main tunnels, as they are driven by shield TBMs with limited insights on the geology surrounding the tunnels (Reinhold et al. 2017; Bergmeister 2019). For the excavation of the ET a hard-rock gripper TBM with a cutterhead diameter of 7.93 m has been used, amongst others equipped with a roof shield with independently movable right- and left cylinders which indirectly indicate rock load variations (Flora et al. 2019). These shields are extended against the overlying rock mass during TBM non-advance periods (TBM standstills), to provide protection for the machinery and the personal in the first four free standing meters behind the tunnel face (Figs. 1 and 2). As the rock mass is applying load on the roof supporting shields, the hydraulic system within the roof support cylinders (RSC), is keeping the shields in place and the pressure in the cylinders is increasing proportionally to the rock load increase. Therefore, the rock load has to be at least of the same amount as the counter pressure in the RSC's deducting the shields dead weight. Whereas during ordinary advance of the TBM the RSC's remain in zero position, leaving

an annular gap of 10 cm between the roof supporting shield and the overlying rock mass, resulting in no greater loads in the RSC's than the shield's dead weight (i.e. base pressure) and eventually the load of some loosened rock fragments resting on it. The pressure threshold of the RSC's is limited to 420 bar to avoid overloading. For loading conditions where the upper limit is reached, stepwise retraction and depressurization take place. In accordance with the TBM manufacturer, to analyse the maximum rock load acting on the TBM's shield, this threshold has been raised to 500 bar during some standstills. Nevertheless, the pressure reached 500 bar and would have climbed on if the over pressure valves of the RSC's would not have prevented it.

## 2.2 Rock Mass Conditions

From North to South the 16.7 km long ET Ahrental-Pfons intersects two main lithological units. It starts in the Quartz Phyllites of Innsbruck, which is a low grade metamorphic phyllite of the Lower Austro-Alpine units, and then penetrates the Bündner Schists of the north-western corner of the Tauern Window (Töchterle 2013; Töchterle and Reinhold 2013) (Fig. 3).

The main foliation of both lithological units dips roughly to the West with varying inclinations between flat and steep. Looking in advance direction of the

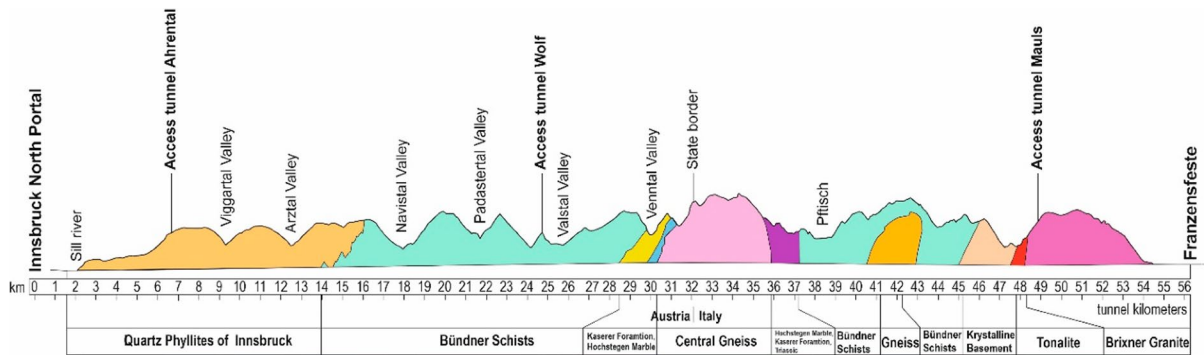


**Fig. 3** Simplified geological cross section through the Brenner Base tunnel, taken from Voit and Kuschel 2020

tunnel, the main foliation is therefore mostly dipping to the right (Flora et al. 2019).

A construction site specific rock mass behaviour classification system—called Geological Indication (GI)- which is based on geological documentation, evaluation of machine parameters, probe drilling and seismic investigation was developed by (Reinhold et al. 2017). The GI-system is of qualitative nature and can be compared to other classifications system e.g. rock mass behaviour type classification (OEGG 2013). The classification comprises four classes (Table 1), where GI 1 refers to good rock mass quality with minor discontinuity-based influence and small deformations; GI 2 indicates rock mass with unfavourable discontinuity intersections or minor faults respectively small deformations; GI 3 stands

for squeezing rock mass, highly fractured rock mass, fault zones and high deformations; and GI 4 describes big, geotechnically relevant (core-) fault zones with very high deformations.

Additional investigation of geological site characterizations provides detailed information about geotechnical conditions on a smaller scale. Regarding the surface conditions of discontinuities, joints feature more favourable (i.e. rougher) surfaces than foliation-, fault- and slickenside planes. It is generally observed that the foliation is acting as one of the most important weakness planes and also generates a penetrating anisotropy within the rock mass.

Outside larger fault zones, the system behaviour (OEGG 2013) on the one hand is influenced by the spacing and orientation of other discontinuities such

**Table 1** Construction site specific rock mass behaviour classification system after Reinhold et al. 2017

Rock mass class (GI)	Short description	Profile maintenance	Deformation
1	Good rock mass, with minor interface influence	Very good, only isolated small-volume outbreaks due to structure	Slight, isotropic <2%
2a	Good rock mass without fault influence, but with unfavourable interface intersections, not squeezing	Good, outbreaks due to structure and induced by gravity	Slight, isotropic <5%
2b	good rock mass with minor fault influence, competent rock	Moderate, also large-volume outbreaks due to structure and induced by gravity, no rock mass pressure	Slight, anisotropic <5%
3	Squeezing rock mass, high degree of fracturing (parallel to schistosity), weakened rock	Moderate, also large-volume outbreaks due to structure, clear sliding at the interfaces due to rock mass pressure	Large to very large, anisotropic 5–10%
4	Rock mass in geotechnically heavily relevant fault zones	Poor, massive large-volume outbreaks	Very large, anisotropic >10%

as faults and fissures and on the other hand by the orientation and arrangement of the foliation. Flora et al. 2019 stated that between these structural elements, the following two relationships can be observed:

- “Increased frequency of fault-occurrence parallel to the main foliation, the foliation as pre-existing weak zone plays a significant role for the formation of brittle faults.”
- “In areas subjected to increased tectonic deformation, softening along the foliation planes is often observed. In vicinity of major faults, part of the tectonic movement occurred through simple shearing along the foliation surfaces.”

### 2.3 Primary Stress-State

According to Braun and Reinhold (2016) the in-situ stresses at the BBT are influenced by a large-scale N-S to NNW-SSE directed stress field resulting from movement on a plate tectonic scale, perpendicular to the arch of the Alps. The local/small scale stress field however, is heavily influenced by the relief of the terrain and therefore highly variable. Some of these variations, documented multiple times by construction site geologists, occur where the tunnel alignment crosses some major regional hill sides, resulting in significantly higher horizontal stresses than vertical stresses (e.g. between tunnel meter 700 and 1100). The overburden in the studied area of the ET varies between 600 and 1000 m.

## 3 Methodology

To be able to analyse the rock loads based on the TBM non advance data, a novel approach of unsupervised ML based data pre-processing was used (chapter 3.1) and a new indicator parameter is developed (chapter 3.2).

### 3.1 Data Pre-Processing

As given in the introduction, the roof support shield passively records differential loading of the overlying rock mass. The goal of pre-processing is to filter out continuous periods of uninterrupted loading of the shields. Problematically, these loading periods

do not simply occur before and after each complete stroke of the TBM, but due to intermediate stops during the excavation process, each stroke is (seemingly) randomly divided into sub-strokes of unequal length. Figure 4 gives an example of the whole stroke number 2368 which is separated into five sub-strokes. A blurred analysis would result if the whole stroke was treated as one instead of separating it into sub-strokes.

As throughout the whole tunnel excavation thousands of these sub-strokes would need to be separated, data pre-processing has the goal to achieve a best fitting separation in a fully automated way as manual filtering would be infeasible. The pre-processing pipeline consists of the following steps: 1. raw data and setting up of a database, 2. filtering out the non-advance periods, 3. correcting the pressures for the “base pressure”, 4. separating sub-strokes via cluster analysis.

#### 3.1.1 Raw Data

TBM operational data was provided by the BBT SE organized as.csv (comma-separated values) files, containing typical TBM operational data (e.g. advance force, cutterhead torque etc.) as well as the recording of the RSC pressures. The data is logged on a ten second basis, resulting in several millions of rows of raw data. In a first step, to provide a clearly arranged, easily accessible and further processable dataset, the raw data has been organized in databases using PostgreSQL (The PostgreSQL Global Development Group, 2020). This open source relational database system allows to handle a wide range of data structuring work, before feeding the data for further investigation via the Psycopg2 adapter (PostgreSQL driver for python; (Varrazzo, 2020)) to the Anaconda Python distribution (Anaconda Inc., 2020).

#### 3.1.2 Filtering for Non-Advance Periods

As described in chapter 2.1 the roof support shield is only extended against the rock mass during stand-stills of the TBM. Therefore, one major prerequisite to obtain continuous and especially stationary loading conditions was to extract the non-advance periods from the raw data. This has been achieved by filtering the raw data for periods where the operational machine parameters: *advance speed*, *advance force* and *penetration* equal to zero, resulting in a

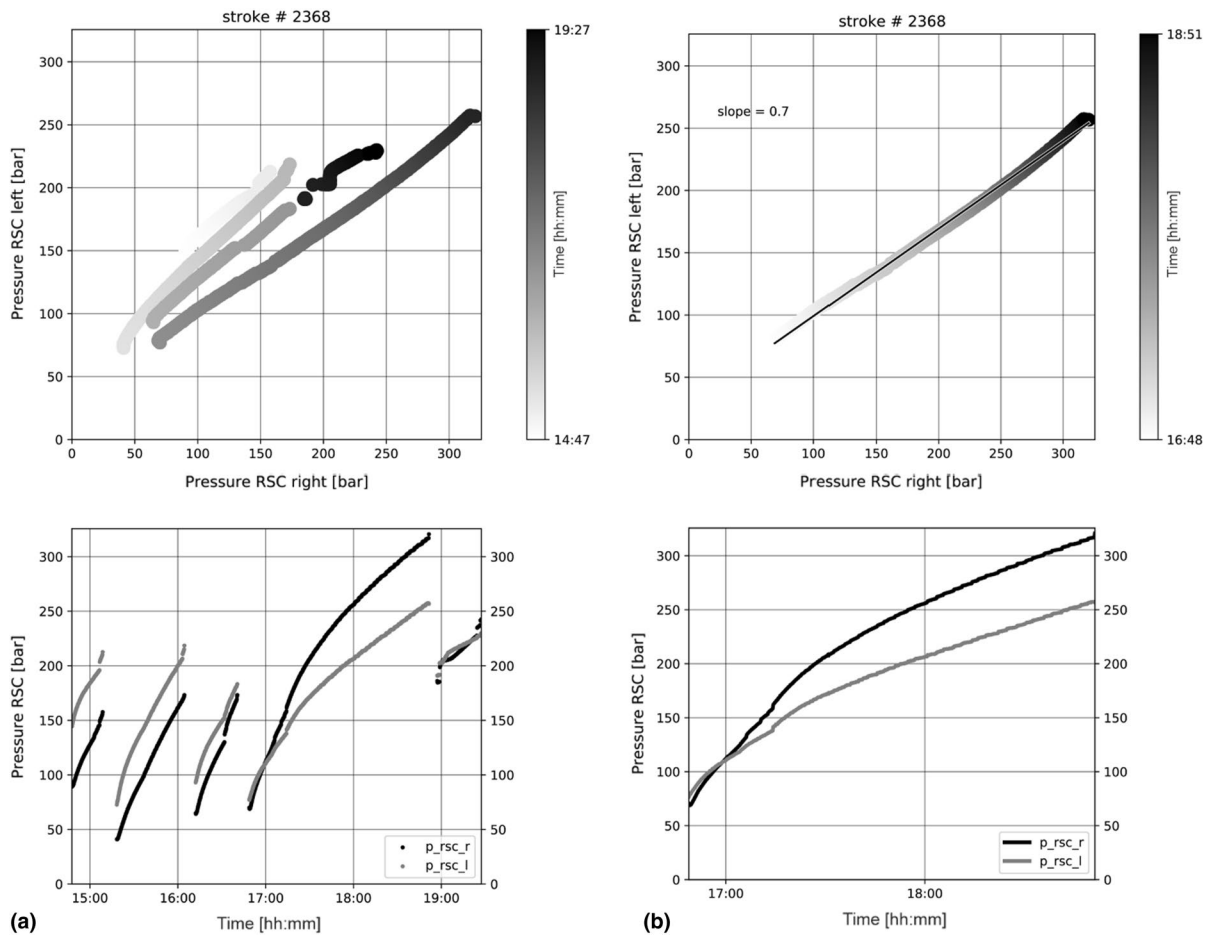


**Fig. 4** Plot of stroke # 2368, in the upper row the pressures in the RSCs left and right have been plotted against each other, whereas in the lower row the pressures were plotted against time (“p\_rsc\_r” and “p\_rsc\_l” denotes the pressure in the right

and left cylinder respectively). The left column shows (Fig. 4a) all pressure increases during stroke 2368 and the right column (Fig. 4b) only shows the longest increase

new database composed solely of data logged during TBM standstills.

### 3.1.3 Base Pressure Revision

To get rid of the shield’s dead weight as a component of the load displayed in the pressure readings of the RSC’s, the next step consisted of a base pressure revision for the whole dataset. According to the manufacturer’s specifications, the base pressure amounts to about 25 bar, calculated from the weight of the roof supporting shield and the attached side panels (Fig. 1). Double checking the calculated base pressure with the logged base pressure obtained from advance periods during operation with an existing annular gap

between the shield and the surrounding rock mass, revealed large deviations for the left RSC, increasing with the length of tunnel. E.g. between tunnel meter 8000 and 9000 the base pressure in the left RSC surpasses the base pressure in the right RSC by 30 bar (Fig. 5a). To overcome this potential instrumental error, first the fluctuation range of the base pressure in the left RSC for every 1000 tunnel meters has been assessed. In a second step for every pressure reading of the RSC’s in the designated fluctuation range, the relative base pressure has been calculated (Eq. 1)

$$rel \cdot BP = BPRSC_{left} - BPRSC_{right} \quad (1)$$

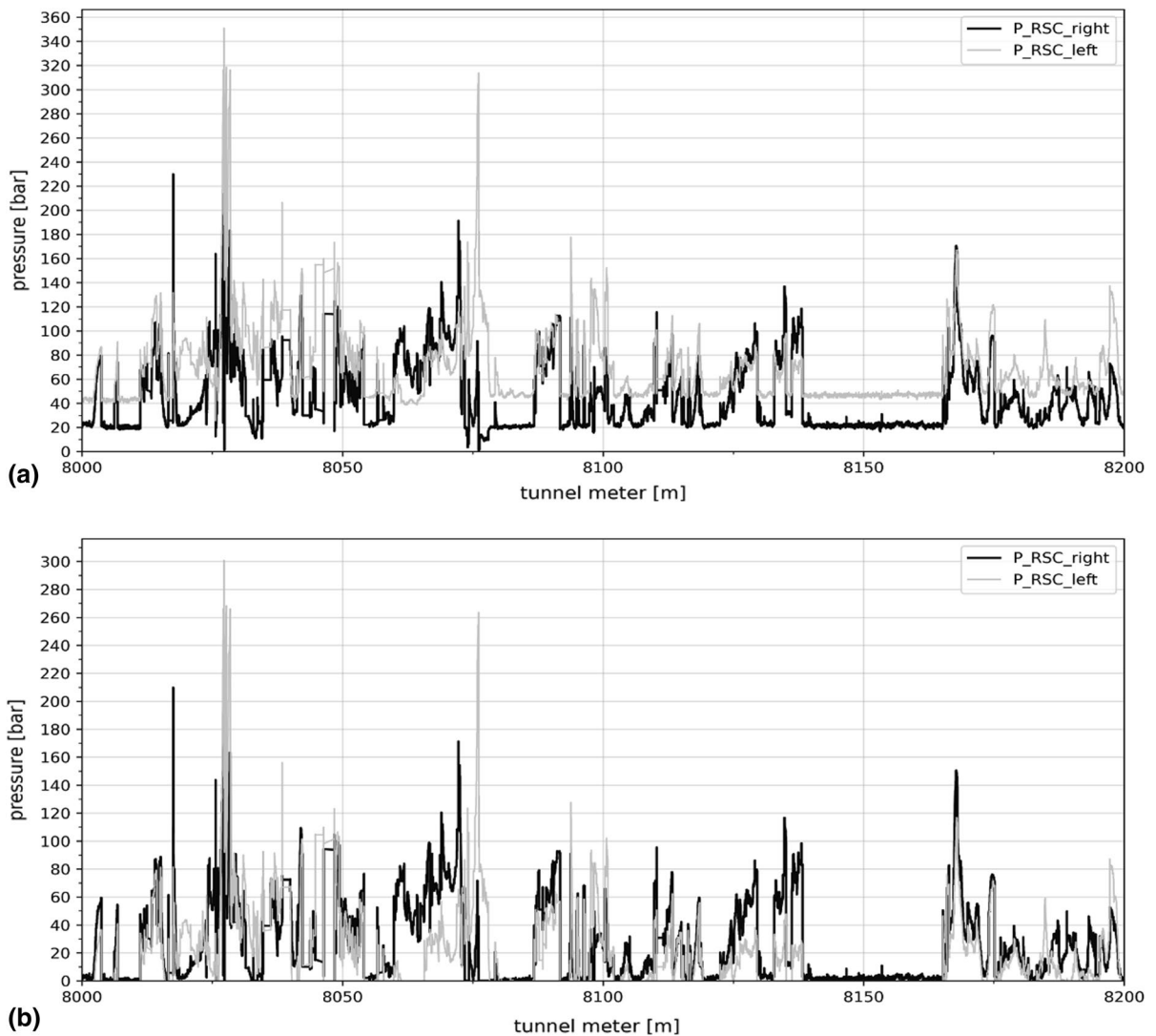


**Fig. 5** Pressure in the RSC’s and the corresponding path of the left RSC from tunnel meter 8000 to 8200, logged during advance periods of the TBM. Figure 5a displays the pressure in

the RSC’s before the base pressure revision, with a clear offset in base pressure between the right and the left RSC. Figure 5b represents the pressure readings after the revision

with  $BPRSC_{left}$  as the base pressure in the left RSC for a single logging entry lying within the fluctuation range and  $BPRSC_{right}$  as the corresponding base pressure of the right RSC. The relative base pressure  $rel.BP$  than got arithmetically averaged over 1000 m. In order to correct the error, the mean relative base pressure  $rel.BP_{mean}$  together with the pressure of the shield’s dead weight  $P_{shield}$  (25 bar), has been subtracted from every initial pressure reading in the left RSC (Eq. 2)

$$P_{RSC_{initial}} - (rel \cdot BP_{mean} + P_{shield}) = P_{RSC_{left_{revised}}} \quad (2)$$

Finally, the pressure of the shields dead weight has also been subtracted from every initial pressure reading of the right RSC  $P_{RSC_{right}}$  (Eq. 3), leaving the dataset adjusted for the impact of the instrumental error and the pressure caused by the shields dead weight (Fig. 5b).

$$P_{RSC_{right}} - P_{shield} = P_{RSC_{right_{revised}}} \quad (3)$$

### 3.1.4 Cluster Analysis/Separation of Sub-Stroke

To separate the sub-strokes, the Scikit-Learn (v. 0.22.1; (Pedregosa et al. 2011)) implementation of the clustering algorithm OPTICS (Ordering Points To Identify the Clustering Structure; (Ankerst et al. 1999)) was used. OPTICS is based on the DBSCAN algorithm (Density-Based Spatial Clustering of Applications with Noise; (Ester et al. 1996)) but improved in such a way that it can better deal with clusters of variable density. Therefore the OPTICS algorithm finds core samples of high density and expands clusters from them (Ankerst et al. 1999). Initial application of both algorithms showed better results for the OPTICS implementation in terms of sub-stroke separation.

To further improve the clustering results and as a consequence thereof, some of the OPTICS default parameters have been changed (Table 2). Changes have been carried out in a way, that for the bigger part of the strokes only one cluster, namely the cluster with the biggest density of data points corresponding to one continuous pressure increase (sub stroke) gets extracted. Besides leaving some parameters on default, this has been realized by increasing the minimum steepness on the reachability plot that constitutes a cluster boundary ( $\xi$ ) as well as increasing the number of samples in a neighbourhood for a point to be considered as a core point ( $min\_samples$ ). Additionally, the minimum number of samples presented by an OPTICS cluster has been set to 360 (one sample every ten seconds; 360 samples are equivalent to one hour), to avoid inclusion of strokes which contain solely short lasting sub-strokes and are too short to display any significant trend. An example for a singled out sub-stroke as a result of the OPTICS clustering algorithm is given in Fig. 4b.

**Table 2** Change of default parameters during the OPTICS cluster analysis

Parameter	Default value	Used value
$\xi$	0.05	0.15
Min_samples	5	25
Min_cluster_size	None	360

### 3.2 Line of Isotropic Pressure (LIP)

After pre-processing, continuous pressure increases for each RSC per sub-stroke during standstills of the TBM are isolated. In order to do a proper comparison between both RSC's and to take qualitative statements about the stress redistribution/direction in the interface between shield and rock mass, the Line of Isotropic Pressure (LIP) was developed.

Plotting the pressures of the left and the right RSC against each other for an isolated sub-stroke (e.g. Figure 4b upper plot), an isotropic pressure increase would represent a straight line of 45°, indicating an equal pressure increase in both cylinders (Fig. 6). In other words, when fitting a linear regression to the aforementioned plot, the LIP would compare to a regression line with a slope equal to 1. Deviations from the LIP towards the horizontal, corresponding to a decrease in slope equal to values < 1, indicate that the pressure increase in the right RSC exceeds the pressure increase in the left cylinder. Same concept applies to deviations from the LIP towards the vertical, corresponding to an increase in slope equal to values > 1, indicating that the pressure increase in the left RSC exceeds the pressure increase in the

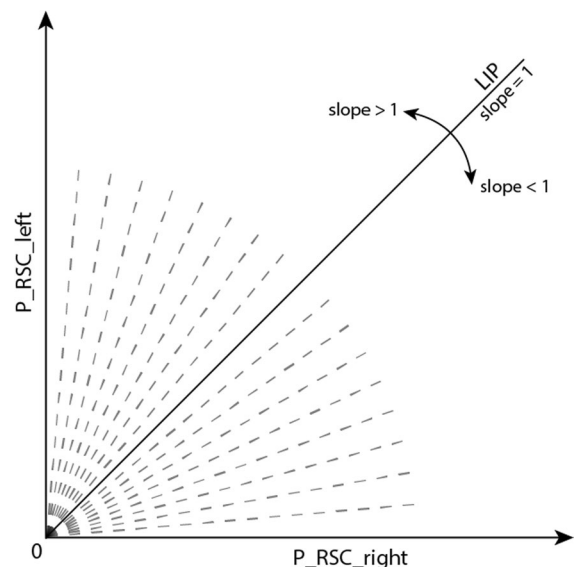


**Fig. 6** Conceptual diagram explaining the Line of Isotropic pressure (LIP): Plot of the pressure in the right RSC on the x-axis vs. the pressure in the left RSC on the y-axis. The LIP corresponds to a linear regression line with a slope of 1 and represents an isotropic increase in pressure in both cylinders



right cylinder. Hence, to assign a slope value to every cluster an extension to the cluster analysis code has been adapted, fitting a linear least squares regression to every cluster/isolated sub-stroke. Over the course of the regression analysis the correlation coefficient has been calculated for every sub-stroke and only sub-strokes displaying a linear relationship between the pressures in both RSC's (correlation coefficient between -0.1 and 0.1) have been taken into consideration for further analysis.

### 4 Results

By means of the cluster analysis based data pre-processing it was possible to single out 5139 significant sub-strokes out of 9105 strokes (for filtering and clustering methods see chapters 3.1 and 3.2). Subsequent investigation of the sub-strokes revealed three recurring patterns of pressure increases. In the first

example (Fig. 7, first column, stroke 634) a nearly isotropic pressure increase can be observed, indicating that the pressure applied on the shield is nearly identical on both sides. For the second example (Fig. 7, second column, stroke 651) the pressure increase in the right RSC surpasses the pressure increase in the left RSC, resulting in a slope < 1. The opposite case, where the pressure increase in the left RSC surpasses the right RSC, is shown in Fig. 7 third column, stroke 2378. Following the approach that the pressure in the RSC's increases with the same extend as the rock load increases, one can state that the rock load acting on the one side of the shield with the higher pressure reading, exceeds the load applied to the shields other side.

The histogram of Fig. 8 represents the distribution of every slope value, obtained by regression analysis applied to every significant continuous pressure increase. The distribution of slopes has a median of 0.71; 68.13% of slopes are <LIP and 31.87%

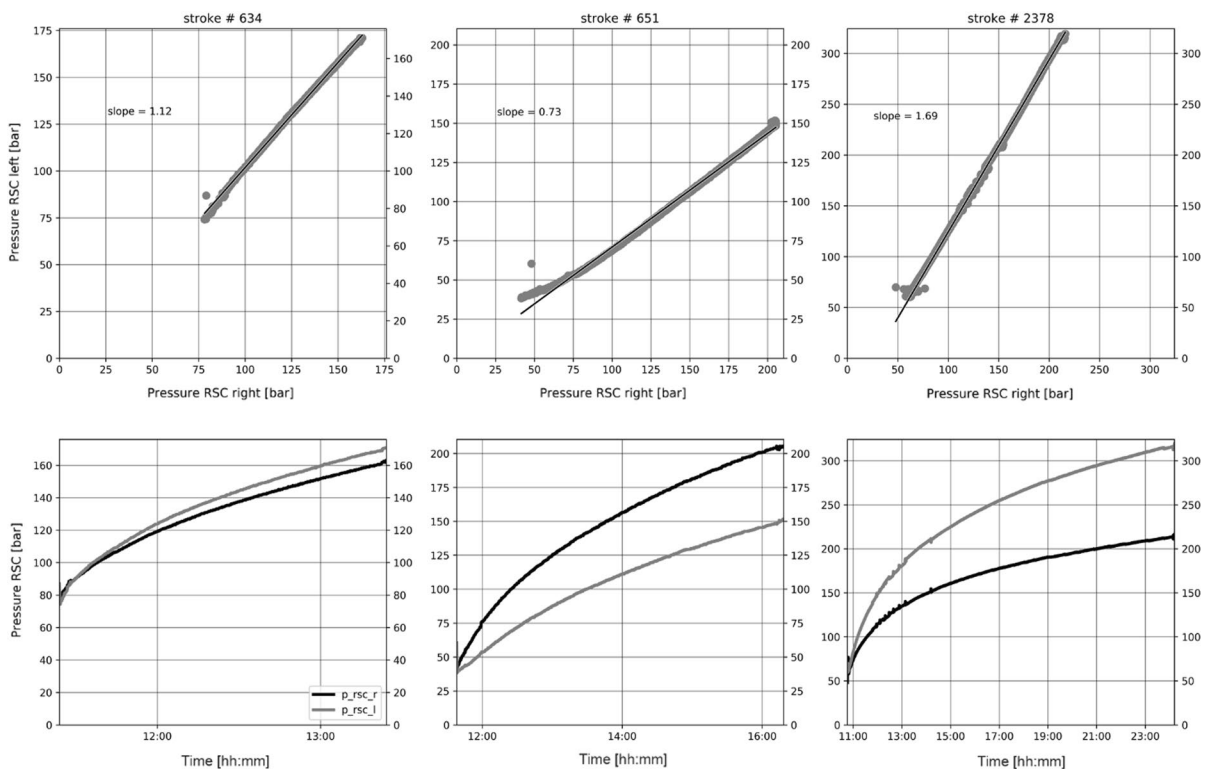


**Fig. 7** Recurring pressure increase patterns, in the upper row of the diagram the pressure in the RSC's is plotted against each other, whereas in the lower row the pressure is plotted against time. First column stroke: # 634 pressure right RSC

nearly equals to the pressure in the left RSC, corresponding to a slope of about 1. Second column: stroke # 651 pressure right RSC > pressure left RSC, slope < 1. Third column: stroke # 2378 pressure right RSC < pressure left RSC, slope > 1

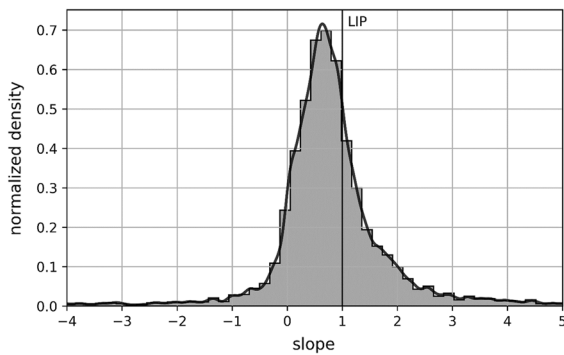


**Fig. 8** Distribution of slopes resulting from a linear regression analysis with a correlation coefficient  $< -0.1$  and  $> 0.1$ . The distribution's median is at 0.71 and 68.13% are  $<$  than the LIP and 31.87% bigger than it

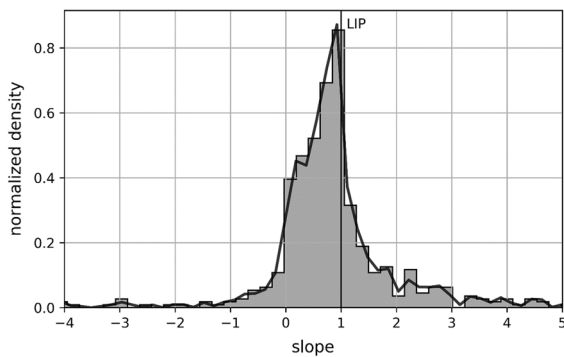


**Fig. 9** Distribution of slopes from a linear regression analysis with a correlation coefficient  $< -0.1$  and  $> 0.1$ , for a particular tunnel section between tunnel meters 735–1120, ( $n = 246$ ). The distribution's median is at 0.82 and 77.64% are  $<$  than the LIP and 22.36% bigger than it

are  $>$  than the LIP. This distribution shows that the right RSC was generally exposed to higher loads throughout the whole tunnel drive.

Referring to geological site characterizations and Bergmeister et al. (2012), in several dedicated areas of the tunnel the initial horizontal stress surpasses the vertical stress in terms of magnitude. The same procedure as explained above has been applied to some of these particular areas. Figure 9 shows the corresponding distribution of slopes for tunnel meter 735 to 1120, obtained from 246 continuous pressure increases. The corresponding distribution of slopes has a median of 0.82, 77.64% of slopes are  $<$  LIP and 22.36% are  $>$  LIP. Regardless of the initial stress

conditions, it is shown that the right RSC is again exposed to a generally higher rate of increasing pressure. Indicating the same anisotropic loading conditions as for the initial stress situation where the vertical stress exceeds the horizontal stress.

## 5 Discussion

There are various publications investigating the anisotropic behaviour of rock masses in tunnelling, most of them based on theoretical 2D and 3D numerical models. In the following section two of them are compared to our on-site derived results.

Fortsakis et al. (2012) stated that the parts of internal rock mass in a circular underground opening behave as a beam, since the discontinuities allow sliding between them. In their models the maximum convergence is developed at the areas where the stratification is tangential to the tunnel section. Applying the beam effect to the ET and considering the above mentioned geological background, this would result in settlements in the right-hand spring line and consequently to an increased load in the right RSC (Fig. 10). The results of this paper are therefore in good agreement with (Fortsakis et al. 2012) as the load concentration in the right RSC ( $<$  than LIP) go along with a foliation that mainly dips to the right (seen in direction of the excavation).

Another study done by Dávila Méndez (2016) shows the influence of dip direction and dip angle of a weakness plane (e.g. foliation) on the displacements of layered rock masses in tunnelling. For the case of the ET where foliation displays a mostly consistent dip direction (seen from the advance direction) mostly dipping to the right, the 3D numerical models of Dávila Méndez would indicate displacements in the right hand spring line and heave in the left hand invert (Fig. 11). Failure is displayed as shearing along the weakness planes (brightest elements in Fig. 11), with the displacement vector rotating against the excavation starting at a dip angle of  $20^\circ$  up to a maximum rotation for a dip of  $50^\circ$ . For this numerical model the Mohr–Coulomb failure criterion was used, additional information on the set boundary conditions can be found in (Dávila Méndez, 2016). Comparing the pressure in the RSC's with the corresponding orientation of the discontinuities, the observed pressure patterns of this paper are in good agreement with the

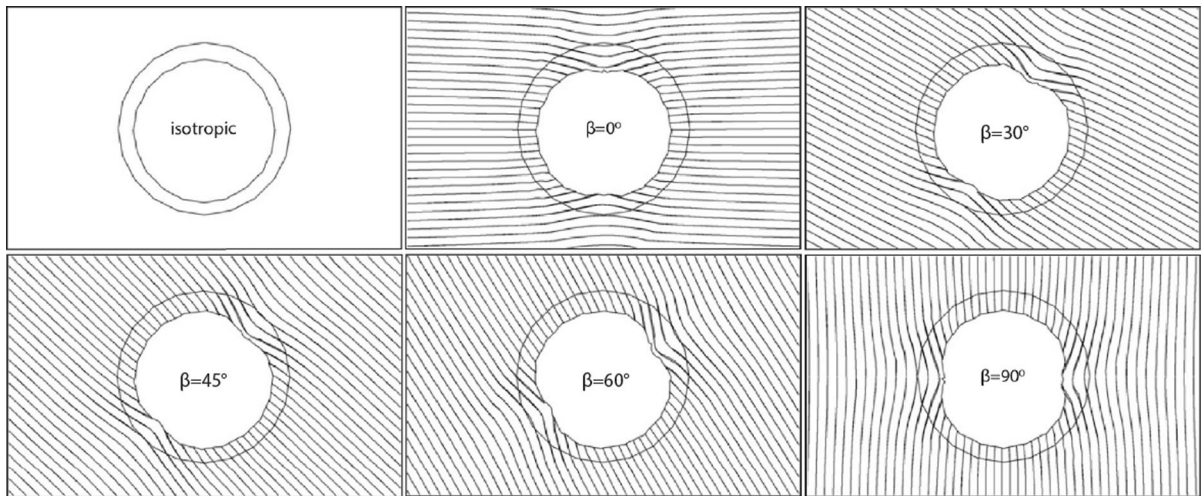
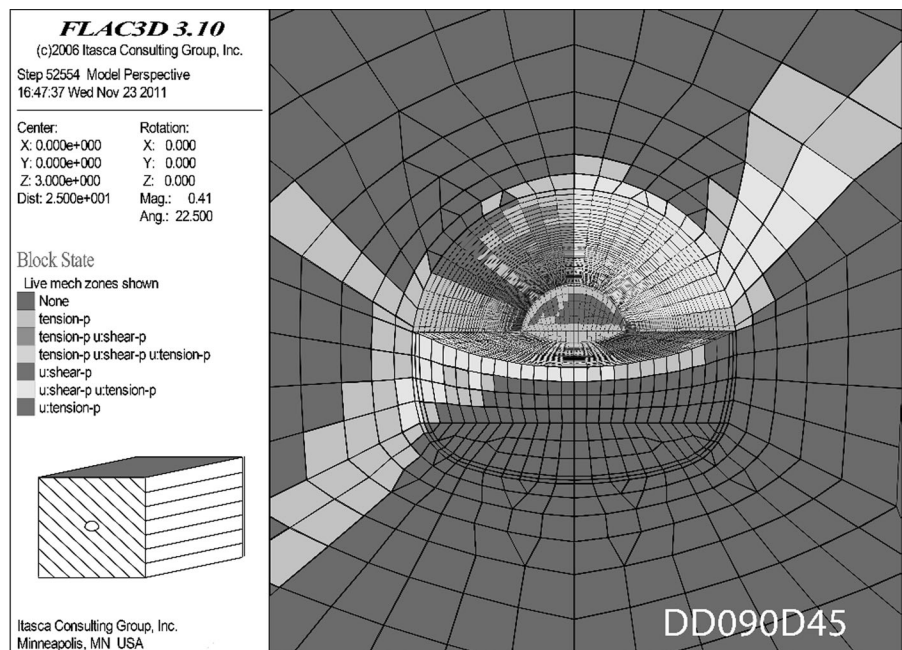


**Fig. 10** Deformed tunnel section from characteristic numerical analysis performed by Fortsakis et. al., 2012 for various bedding angles ( $\beta$ ) of persistent discontinuities. (After Fortsakis et. al., 2012)

**Fig. 11** 3D numerical model showing the displacements for major weakness planes with a dip direction normal to the direction of drive and a dip of 45°. (After Dávila Méndez, 2016)



displacement patterns one would expect considering the approach of Dávila Méndez. This applies especially for tunnel sections where only one discontinuity set is dominant (Fig. 12).

On the other hand, Kluckner and Schubert (2019) did a study at the Semmering Base Tunnel, investigating anisotropic displacement patterns of fine grained phyllites. According to them, in geomechanics

primary anisotropy can be either due to geological structures geomechanically effective (e.g. well-developed foliation) or due to the direction of the primary stress field. Furthermore, they found that the effect of the foliation on the displacements depends on how well the foliation is developed, therefore for more fragmented rock masses (i.e. closer foliation—and/or joint spacing) the effect of the foliation

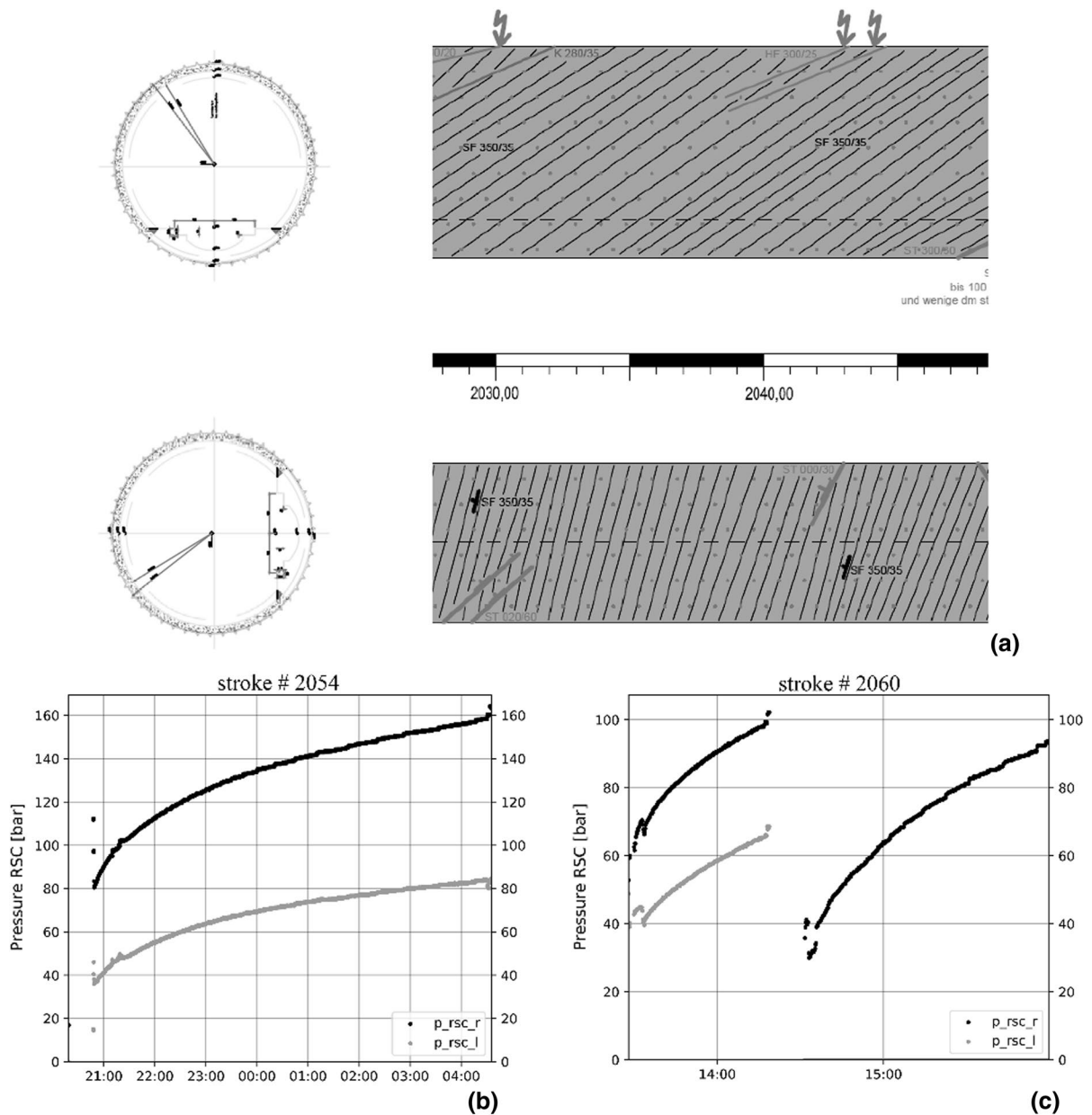


**Fig. 12** Graphically illustrated tunnel section with corresponding pressure in the RSC's. The upper part in Fig. 12a represents a longitudinal section at the tunnel axis and the lower part a horizontal section at vertical alignment level, both illustrated with dip direction/dip of encountered discontinuities.

is higher. However, in rock masses showing a low strength-stress ratio, and a wider foliation—and/or joint spacing, the effect of the orientation of the primary stresses has more influence on the displacements. Considering the higher load in the right RSC

ties. Figure 12b shows the pressure increase patterns for both RSC's left and right for stroke # 2054, between tunnel meters 2035.18–2036.90. The same applies to Fig. 11c for stroke # 2060, between tunnel meters 2043.76–2045.38

in general and through zones where the horizontal stress surpasses the vertical stress, it seems that for the exploratory tunnel the foliation has a much bigger influence on the load applied on the shield, then the orientation of the primary stress field.

## 6 Conclusion and Outlook

TBM operational data continuously logged over a tunnel length of 15 km has been digitally pre-processed, clustered and investigated. The paper at hand analysed how monitored roof supporting cylinder pressures can be used to qualitatively describe the stress redistribution/direction in the interface roof supporting shield to rock mass. To do so a pre-processing workflow based on cluster analysis was developed and a new concept to determine the loading situation in the RSC's, the line of isotropic pressure, has been introduced.

Considering the system behaviour and the above presented loading conditions, the observed deformations confirm that the foliation is the weakest plane within the discontinuities. Furthermore, its orientation and arrangement highly impact the direction and amount of load the TBM's roof-supporting shields are exposed to. Comparison of the above presented, directly investigated RSC loading conditions with various studies based on empirical, analytical and numerical models, shows good agreement with regard to the displacement of anisotropic layered rock masses in underground openings.

Furthermore, it has been demonstrated that after some pre-processing steps, the load in the RSC's suits the purpose as an exploratory tool, in terms of stress redistribution/direction, very well. Continuous logging of machine parameters made it possible to not only investigate dedicated tunnel sections, but to make conclusions on the system behaviour considering the whole tunnel length. Together with the site characterization mapped by engineering geologists, the pressure in the RSC's could provide a vital parameter to better understand the overall system behaviour, influencing many parts of the tunnelling process.

In order to quantitate the rock load acting on the TBM's shield, attempts to back calculate the pressure recorded in the RSC's have been made, but qualitative description is limited by the fact that the RSC's only operate in a certain pressure threshold (for details see chapter 2.1). Future studies in collaboration with TBM manufacturers, contractors and clients should address this problem and yield insights to rock loads in general and stress redistributions and relaxations during mechanized tunnel drives in particular.

**Acknowledgements** The BBT SE is gratefully acknowledged for providing data from the exploratory tunnel Ahrental-Pfons.

**Funding** Open access funding provided by Graz University of Technology. This research did not receive any specific grant from funding agencies in the public, commercial, or not-for-profit sectors.

**Availability of data and material** The datasets generated during and/or analysed during the current study are not publicly available due to a confidentiality agreement with the BBT SE.

**Code availability** The Python code used for data pre-processing and plotting of figures can be accessed via the following link:<https://github.com/paulunl/Python-Code-Masterthesis.git>

**Declarations**

**Conflicts of interest** Not applicable.

**Open Access** This article is licensed under a Creative Commons Attribution 4.0 International License, which permits use, sharing, adaptation, distribution and reproduction in any medium or format, as long as you give appropriate credit to the original author(s) and the source, provide a link to the Creative Commons licence, and indicate if changes were made. The images or other third party material in this article are included in the article's Creative Commons licence, unless indicated otherwise in a credit line to the material. If material is not included in the article's Creative Commons licence and your intended use is not permitted by statutory regulation or exceeds the permitted use, you will need to obtain permission directly from the copyright holder. To view a copy of this licence, visit <http://creativecommons.org/licenses/by/4.0/>.

## References

- Anaconda Inc., 2020. anaconda.com [WWW Document]. URL <https://www.anaconda.com/> (accessed 9.17.20)
- Ankerst M, Breunig MM, Kriegel H, Sander J (1999) OPTICS: Ordering points to identify the clustering structure. ACM SIGMOD Record 28:49–60. <https://doi.org/10.1145/304181.304187>
- Bach D, Holzer W, Leitner W, Radončić N (2018) The use of TBM process data as a normative basis of the contractual advance classification for TBM advances in hard rock. Geomech Und Tunnelbau 11:505–518. <https://doi.org/10.1002/geot.201800042>
- bbtinfo.eu [WWW Document], 2020. URL <https://www.bbtinfo.eu/> (accessed 9.25.20)
- BBT-SE.com [WWW Document], 2020. URL <https://www.bbt-se.com/> (accessed 9.24.20)
- Bergmeister K (2019) The Brenner Base Tunnel – geological, construction and logistical challenges and innovations at half time Der Brenner Basistunnel – geologische,

- bautechnische, logistische Herausforderungen und Innovationen zur Halbzeit. *Geomech Und Tunnelbau* 12:555–563. <https://doi.org/10.1002/geot.201900038>
- Bergmeister K, Reinhold C (2017) Lernen und Optimieren vom Erkundungsstollen – Brenner Basistunnel. *Geomech Und Tunnelbau* 10:467–476. <https://doi.org/10.1002/geot.201700039>
- Bergmeister K, Weifner T, Collizzollo M (2012) Auswirkungen der geometrischen Lage der Tunnel auf die Gebirgsplastifizierung und die Spritzbetonschale beim Brenner Basistunnel. *Beton- Und Stahlbetonbau* 107:735–748. <https://doi.org/10.1002/best.201200059>
- Braun R, Reinhold C (2016) Determination of the 3D in situ stress conditions for the geotechnical planning and the construction of the Brenner Base Tunnel. 45. *Geomech. Kolloquium Der Tech Univ Bergakademie Freib* 2:183–204
- Dávila Méndez JM (2016) Displacements analysis in layered rock masses. Graz University of Technology, UK
- Entacher M, Winter G, Bumberger T, Decker K, Godor I, Galler R (2012) Cutter force measurement on tunnel boring machines - System design. *Tunn Undergr Sp Technol* 31:97–106. <https://doi.org/10.1016/j.tust.2012.04.011>
- Erharder GH, Marcher T, Reinhold C (2019b) Application of artificial neural networks for Underground construction – Chances and challenges – Insights from the BBT exploratory tunnel Ahrental Pfans. *Geomech Und Tunnelbau* 12:472–477. <https://doi.org/10.1002/geot.201900027>
- Erharder GH, Marcher T, Reinhold C, 2019a. Comparison of artificial neural networks for TBM data classification, In: *Rock mechanics for natural resources and infrastructure development- proceedings of the 14th international congress on rock mechanics and rock engineering*, ISRM 2019a. CRC Press/Balkema, pp. 2426–2433
- Erharder GH, Marcher T, Reinhold C, (2020) Artificial neural network based online rockmass behavior classification of TBM Data, In: *Springer Series in Geomechanics and Geo-engineering*. Springer, pp. 178–188. [https://doi.org/10.1007/978-3-030-32029-4\\_16](https://doi.org/10.1007/978-3-030-32029-4_16)
- Ester M, Kriegel H, Xu X, Miinchen D. (1996). A density-based algorithm for discovering clusters in large spatial databases with noise. *Int Conf Knowl Discov Data Min.* 6.
- Festa D, Broere W, Bosch JW (2012) An investigation into the forces acting on a TBM during driving - Mining the TBM logged data. *Tunn Undergr Sp Technol* 32:143–157. <https://doi.org/10.1016/j.tust.2012.06.006>
- Flora M, Grüllich S, Töchterle A, Schierl H (2019) Brenner Base Tunnel exploratory tunnel Ahrental-Pfans – interaction between tunnel boring machine and rock mass as well as measures to manage fault zones. *Geomech Tunn* 12:575–585. <https://doi.org/10.1002/geot.201900044>
- Fortsakis P, Nikas K, Marinos V, Marinos P (2012) Anisotropic behaviour of stratified rock masses in tunnelling. *Eng Geol* 141–142:74–83. <https://doi.org/10.1016/j.enggeo.2012.05.001>
- Huang X, Liu Q, Liu H, Zhang P, Pan S, Zhang X, Fang J (2018) Development and in-situ application of a real-time monitoring system for the interaction between TBM and surrounding rock. *Tunn Undergr Sp Technol* 81:187–208. <https://doi.org/10.1016/j.tust.2018.07.018>
- Kluckner A, Schubert W, (2019). Study on the anisotropic displacement pattern at a conventional tunnel drive. *ISRM 2019 Spec. Conf*
- Li S, Feng X, Li Z, Chen B, Jiang Q, Wu S, Hu B, Xu J (2011) In situ experiments on width and evolution characteristics of excavation damaged zone in deeply buried tunnels. *Sci China Technol Sci* 54:167–174. <https://doi.org/10.1007/s11431-011-4637-0>
- Marcher T, Erharder GH, Winkler M (2020a) Machine Learning in tunnelling – Capabilities and challenges. *Geomech Und Tunnelbau* 13:191–198. <https://doi.org/10.1002/geot.202000001>
- Marcher T, Sackl G, Reinhold C, 2020b. using gripper forces of an open gripper TBM to evaluate rock mass stiffness. *ARMA Proc*
- OEGG, 2013. Richtlinie für die geotechnische Planung von Untertagebauten mit kontinuierlichem Vortrieb 49.
- Pedregosa F, Weiss R, Brucher M (2011) Scikit-learn : Machine Learning in Python. *J Mach Learn Res* 12:2825–2830
- Pilgerstorfer T, Radončić N, Moritz B, Goricki A (2011) Auswertung und interpretation der messdaten aus dem versuchsstollen EKT Paierdorf. *Geomech Und Tunnelbau* 4:423–434. <https://doi.org/10.1002/geot.201100036>
- Ramoni M, Anagnostou G (2006) On the feasibility of TBM drives in squeezing ground. *Tunn Undergr Sp Technol* 21:262. <https://doi.org/10.1016/j.tust.2005.12.123>
- Ramoni M, Anagnostou G (2010a) Thrust force requirements for TBMs in squeezing ground. *Tunn Undergr Sp Technol* 25:433–455. <https://doi.org/10.1016/j.tust.2010.02.008>
- Ramoni M, Anagnostou G (2010) Tunnel boring machines under squeezing conditions. *Tunn Undergr Sp Technol*. <https://doi.org/10.1016/j.tust.2009.10.003>
- Ramoni M, Anagnostou G (2011) The interaction between shield, ground and tunnel support in TBM tunnelling through squeezing ground. *Rock Mech Rock Eng* 44:37–61. <https://doi.org/10.1007/s00603-010-0103-8>
- Ramoni M, (2010) On the feasibility of TBM drives in squeezing ground and the risk of shield jamming. *ETH Zurich*
- Reinhold C, Schwarz C, Bergmeister K (2017) Development of holistic prognosis models using exploration techniques and seismic prediction: Die Entwicklung holistischer Prognosemodelle mit Vorerkundungen und seismischen Messungen. *Geomech Und Tunnelbau* 10:767–778. <https://doi.org/10.1002/geot.201700058>
- Sun W, Shi M, Zhang C, Zhao J, Song X (2018) Dynamic load prediction of tunnel boring machine (TBM) based on heterogeneous in-situ data. *Autom Constr* 92:23–34. <https://doi.org/10.1016/j.autcon.2018.03.030>
- The PostgreSQL Global Development Group, 2020. postgresql.org [WWW Document]. URL <https://www.postgresql.org/> (accessed 9.17.20)
- Töchterle A, Reinhold C, (2013). Ermittlung der geomechanischen Kennwerte von Störungszonen im Innsbrucker Quarzphyllit auf Basis der Erkundungsergebnisse beim Brenner Basistunnel Quarzphyllite based on the exploration results of the Brenner Base Tunnel. 19. Tagung der Ingenieurgeologie München
- Töchterle A, (2013) Brenner Basistunnel: Wichtigkeit der Vorerkundung. *tunnel 01*, 12–23

- Varrazzo, D., 2020. psycogp.org [WWW Document]. URL <https://www.psycogp.org/> (accessed 9.17.20)
- Voit K, Kuschel E (2020) Rock material recycling in tunnel engineering. Appl Sci 10:546. <https://doi.org/10.3390/AP10082722>

**Publisher's Note** Springer Nature remains neutral with regard to jurisdictional claims in published maps and institutional affiliations.